

# Patch-aware Batch Normalization for Improving Cross-domain Robustness

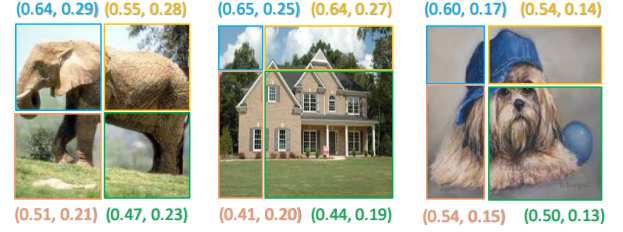
Lei Qi, Dongjia Zhao, Yinghuan Shi, Xin Geng

**Abstract**—Despite the significant success of deep learning in computer vision tasks, cross-domain tasks still present a challenge in which the model’s performance will degrade when the training set and the test set follow different distributions. Most existing methods employ adversarial learning or instance normalization for achieving data augmentation to solve this task. In contrast, considering that the batch normalization (BN) layer may not be robust for unseen domains and there exist the differences between local patches of an image, we propose a novel method called patch-aware batch normalization (PBN). To be specific, we first split feature maps of a batch into non-overlapping patches along the spatial dimension, and then independently normalize each patch to jointly optimize the shared BN parameter at each iteration. By exploiting the differences between local patches of an image, our proposed PBN can effectively enhance the robustness of the model’s parameters. Besides, considering the statistics from each patch may be inaccurate due to their smaller size compared to the global feature maps, we incorporate the globally accumulated statistics with the statistics from each batch to obtain the final statistics for normalizing each patch. Since the proposed PBN can replace the typical BN, it can be integrated into most existing state-of-the-art methods. Extensive experiments and analysis demonstrate the effectiveness of our PBN in multiple computer vision tasks, including classification, object detection, instance retrieval, and semantic segmentation.

**Index Terms**—single-source domain generalization, cross-perturbation, MixPatch.

## I. INTRODUCTION

IN the last decade, deep learning has made significant progress in various applications, including image classification [1, 2, 3, 4, 5], object detection [6], and semantic segmentation [7, 8]. However, most existing deep learning methods assume that the training and test sets are independent and identically distributed (IID), meaning they come from the same data distribution. This assumption is often not satisfied in real-world applications, resulting in poor performance of deep models in cross-domain tasks (*i.e.*, the training and test sets follow different distributions). For example, in urban-scene object detection, the collected images can vary widely depending on weather conditions, making it difficult to collect diverse



(a) Images for classification.



(b) Images for detection and segmentation.

Fig. 1: The illustration of the differences between local patches within an image. We randomly divide each image into four non-overlapping patches and calculate the statistics (mean and standard deviation) of all pixels within each patch. As shown, there are discrepancies between the patches in terms of both statistics and visualization. Motivated by this observation, we propose a novel method called patch-aware batch normalization (PBN) that leverages these differences to improve cross-domain robustness.

images that cover all conditions, especially in unpredictable real-world environments.

In recent years, several domain generalization (DG) methods have been developed to address the issue of cross-domain tasks [9, 10, 11, 12, 13, 14, 15], which involves training a robust model capable of generalizing well to any unseen domains. Most of these methods are based on multiple source domains, meaning that the training set consists of samples from multiple different domains. These methods have achieved a significant improvement in the model’s generalization capability due to the diverse information brought by multiple domain samples. However, it becomes even more challenging when there is only a single-source domain in the training stage, as the lack of intra-domain sample diversity makes it easier for the model to overfit to the training set. In this paper, we focus on exploring the single-source domain generalization (SDG) task.

To tackle the challenge of the single-source domain gener-

The work is supported by NSFC Program (Grants No. 62206052, 62125602, 62076063), China Postdoctoral Science Foundation (No. 2024M750424, GZC20240252), Jiangsu Funding Program for Excellent Postdoctoral Talent under Grant No. 2024ZB242, and the Xplorer Prize.

Lei Qi, Dongjia Zhao, and Xin Geng are with the School of Computer Science and Engineering, Southeast University, and Key Laboratory of New Generation Artificial Intelligence Technology and Its Interdisciplinary Applications (Southeast University), Ministry of Education, China, 211189 (e-mail: qilei@seu.edu.cn; zhaodongjia@seu.edu.cn; xgeng@seu.edu.cn).

Yinghuan Shi is with the State Key Laboratory for Novel Software Technology, Nanjing University, Nanjing, China, 210023 (e-mail: syh@nju.edu.cn).

Corresponding author: Xin Geng.

alization (SDG), some augmentation-based methods have been developed, based on adversarial learning [16, 17, 18, 19] or instance normalization [20, 21], to achieve data augmentation. Additionally, an attention consistency loss is introduced to ensure alignment of class activation maps between original and augmented versions of the same training sample [22]. Moreover, some multi-source domain generalization methods, such as Exact Feature Distribution Matching [9] and Cross-Domain Ensemble Distillation [23], can also be applied to the single-domain task. In contrast to these existing methods, our method focuses on addressing the issue from the perspective of batch normalization (BN).

We have noticed that there are differences between local patches in an image, as shown in Fig. 1. To be specific, we randomly split an image into four non-overlapping patches and compute the statistics, such as mean and standard deviation, for all pixels in each patch. Previous studies have shown that feature statistics can carry style information for an image [24, 25]. As shown in Fig. 1 (b) on the right, the top-left patch differs from the others in terms of both statistics and visualization. We aim to utilize these differences in local patches to enhance cross-domain robustness.

Moreover, several studies have shown that the traditional batch normalization (BN) method is not robust in handling domain shift [26, 27]. BN typically use a pair of statistics to normalize all samples in a batch, and data diversity is lacking in a domain. As a result, we argue that the learnable affine transformation parameters of BN may not be robust in the SDG task. To address this issue, we propose a novel patch-aware batch normalization (PBN) that leverages the differences between local patches in an image to improve the cross-domain robustness. To be specific, we randomly split the feature maps into multiple non-overlapping patches along the spatial dimension in the training stage and perform normalization for each patch independently. This method can better optimize the shared parameter of the normalization layer. Meanwhile, by leveraging the diverse information from PBN, other parameters in the model also become more robust. Besides, the statistics from each patch may not be accurate due to their smaller size compared to the global feature maps.

To overcome this, we combine the globally accumulated statistics with the statistics from each batch to obtain the final statistics for normalizing each patch. It's worth noting that the scheme for the accumulated statistics is the same as that used in typical BN, *i.e.*, it is accumulated by the global feature maps. Since our method is an improved BN scheme for the SDG task, it can be combined with most existing state-of-the-art (SOTA) methods. We conduct extensive experiments on multiple tasks, including classification, object detection, instance retrieval, and semantic segmentation, which verify the effectiveness of the proposed method. Furthermore, ablation studies confirm the efficacy of each component of our patch-aware batch normalization in different tasks.

Our method primarily leverages the diversity in the data distribution between patches of an image. This can be considered as some prior knowledge of each image itself. Compared to adversarial learning methods, the diversity information in our approach is not acquired through learning, and most

adversarial learning methods aim to learn diversity from a vast unknown space, making it difficult to achieve an optimal solution and requiring a balance between preserving semantic information and enhancing information diversity. Additionally, regarding instance normalization methods, the literature [28] has pointed out that they lose semantic information. In contrast, BN has a good ability to retain semantic information. Our method further explores diversity while maintaining the ability to retain semantic information, resulting in better model generalization performance.

## II. RELATED WORK

In this section, we will provide a review of the most relevant studies to our proposed method, including works on multi-source and single-source domain generalization, as well as normalization methods for generalization.

### A. Domain Generalization

Domain generalization is a challenging task in which the goal is to train a model on source domains and ensure that it can generalize well to unseen target domains. Recent studies have made significant progress in this area, including augmentation-based methods, learning domain-invariant features, and meta-learning-based methods. To address the diversity of training samples, *some augmentation schemes* have been proposed to enrich training data [29, 9, 30, 31, 32, 33]. From an optimization perspective, Cha *et al.* [34] theoretically show that finding flat minima leads to a smaller domain generalization gap. Thus, a simple yet effective method called stochastic weight averaging densely has been developed to find flat minima. Lee *et al.* [23] put forward another simple yet effective method called cross-domain ensemble distillation, which *learns domain-invariant features* while encouraging the model to converge to flat minima, recently found to be a sufficient condition for domain generalization. Moreover, *meta-learning* has also been employed to address the DG task, which mimics the source domain and the unseen target domain using the meta-train set and the meta-test set in the training process [10]. The domain-invariant feature is also beneficial for the model's generalization [35, 36, 37, 38].

### B. Single-source Domain Generalization

Single-source domain generalization is a challenging task where models trained with data from only one domain are required to perform well on many unseen domains. To address this, various augmentation methods have been proposed, including both image-level [39, 22] and feature-level [40, 18, 41, 17] techniques. For instance, Chen *et al.* [17] propose a center-aware adversarial augmentation technique that expands the source distribution by altering the source samples to push them away from class centers via an angular center loss. In single-source DG object detection, Wu *et al.* [42] present a method to disentangle single-domain generalized object detection in urban scene via cyclic-disentangled self-distillation, which learns domain-invariant features without the need for domain-related annotations. In contrast to these

methods, Wan *et al.* [43] decompose convolutional features of images into meta-features, which are defined as universal and basic visual elements for image representations.

### C. Normalization for Generalization

Recent research has shown that the statistics of instance normalization (IN) represent the style of images. Therefore, some methods introduce noise information into IN to enhance its robustness [20, 21]. Li *et al.* [21] improve network generalization ability by modeling domain shift uncertainty with synthesized feature statistics during training. Tang *et al.* [44] introduce CrossNorm and SelfNorm. CrossNorm exchanges channel-wise mean and variance between feature maps to increase the training distribution, while SelfNorm uses attention to recalibrate statistics to bridge gaps between training and test distributions. Although CrossNorm and SelfNorm explore different directions in statistics usage, they can complement each other. Zhou *et al.* [45] propose a novel method based on probabilistically mixing instance-level feature statistics of training samples across source domains.

Several domain generalization methods have been developed based on batch normalization. Seo *et al.* [27] use multiple normalization layers and learn separate affine parameters per domain. They normalize activations for each domain by taking a weighted average of batch and instance normalization statistics. Huang *et al.* [46] show that estimation shift can accumulate due to the stack of batch normalization layers in a network, which can hurt test performance. To address this issue, they propose a batch-free normalization method to prevent the accumulation of estimation shift. Fan *et al.* [16] introduce a generic adaptive standardization and rescaling normalization using adversarial learning. In contrast to these methods, we propose an improved batch normalization technique that exploits the differences in local patches within an image to enhance the robustness of the BN’s parameters.

Compared to other existing methods, the advantages of our proposed PBN are as follows: 1) The proposed method introduces the prior information of the diversity of local image regions into BN, which has not been explored in these existing methods. 2) Unlike other methods, our approach ensures the diversity of augmented features without introducing additional noise, effectively preserving the information. 3) Our method can also be combined with other augmentation methods, further enhancing the model’s generalization performance.

## III. METHOD

In this paper, to improve the robustness of cross-domain models, we propose a novel method called patch-aware batch normalization (PBN) to address the overfitting to the source domain via exploiting the differences between local patches within an image. In this section, we will first review the basics of BN and then introduce PBN in detail.

### A. Background

Here, we will review the conventional batch normalization (BN) [47]. First, we define feature maps of a batch as  $f \in$

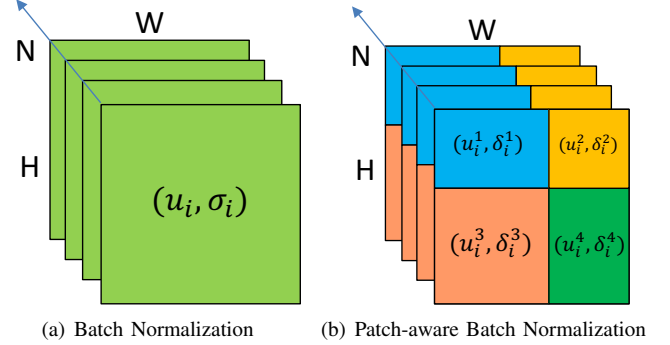


Fig. 2: Comparison between the typical batch normalization (BN) and our patch-aware batch normalization (PBN). These figures show the normalization operation for the  $i$ -th channel. In (b), we assume that feature maps of the  $i$ -th channel are randomly divided into 4 patches.

$\mathbb{R}^{N \times C \times H \times W}$ , where  $N$  and  $C$  are the number of samples and channels, and  $H$  and  $W$  are the height and the width of feature maps. In general, BN leverages a global statistics of a batch to normalize all samples at each iteration, which can be defined as:

$$\text{BN}(f) = \gamma \frac{f - \mu}{\sigma} + \beta, \quad (1)$$

where  $\gamma, \beta \in \mathbb{R}^C$  are learnable affine transformation parameters, and  $\mu, \sigma \in \mathbb{R}^C$  (*i.e.*,  $\mu = [\mu_1, \dots, \mu_C]$  and  $\sigma = [\sigma_1, \dots, \sigma_C]$ ) represent the channel-wise mean and standard deviation (*i.e.*, statistics) of BN for feature maps. For statistics of the  $i$ -th channel are presented as:

$$\mu_i = \frac{1}{NHW} \sum_{n=1}^N \sum_{h=1}^H \sum_{w=1}^W f[n, i, h, w], \quad (2)$$

$$\sigma_i = \sqrt{\frac{1}{NHW} \sum_{n=1}^N \sum_{h=1}^H \sum_{w=1}^W (f[n, i, h, w] - \mu_i)^2 + \epsilon}, \quad (3)$$

where  $\epsilon$  is a constant for numerical stability. In the above equation, it can be observed that BN employs the global statistics of a batch (*i.e.*, a pair of  $\mu$  and  $\sigma$ ) for all samples at each iteration. As a result, the neural network could learn a fixed pattern, which can cause the final model to overfit to the source domain, especially when the training set lacks diversity. Moreover, the values of  $\gamma$  and  $\beta$  in Eq. 1 may not be robust when the test samples do not follow the same distribution as the training samples. In this paper, we propose a novel batch normalization method to address this issue.

### B. Patch-aware BN

In this paper, a novel method called Patch-aware Batch Normalization (PBN) is proposed to address the aforementioned issues of BN. PBN leverages the differences between non-overlapping patches within an image to enhance the robustness of cross-domain models, as shown in Fig. 1. The discrepancy between BN and PBN is illustrated in Fig. 2. In PBN, the

feature maps are split into multiple non-overlapping patches, and each patch is normalized independently during the forward process. We assume that the number of patches is represented by  $P$ , meanwhile  $H_p$  and  $W_p$  denote the height and width of the  $p$ -th patch. We formulate PBN as follows:

$$\text{PBN}(f^p) = \gamma \frac{f^p - \mu^p}{\sigma^p} + \beta, \quad p \in \{1, \dots, P\}, \quad (4)$$

where  $\mu^p, \sigma^p \in \mathbb{R}^C$  (i.e.,  $\mu^p = [\mu_1^p, \dots, \mu_C^p]$  and  $\sigma^p = [\sigma_1^p, \dots, \sigma_C^p]$ ) represent the channel-wise mean and standard deviation (i.e., statistics) of the  $p$ -th patch within feature maps. The statistics of the  $i$ -th channel are written as:

$$\mu_i^p = \frac{1}{NH_pW_p} \sum_{n=1}^N \sum_{h=1}^{H_p} \sum_{w=1}^{W_p} f^p[n, i, h, w], \quad (5)$$

$$\sigma_i^p = \sqrt{\frac{1}{NH_pW_p} \sum_{n=1}^N \sum_{h=1}^{H_p} \sum_{w=1}^{W_p} (f^p[n, i, h, w] - \mu_i^p)^2 + \epsilon}. \quad (6)$$

Although using the method can alleviate the overfitting to the training set,  $H_p$  and  $W_p$  in Eqs. 5 and 6 are smaller than  $H$  and  $W$  in Eqs. 2 and 3 (refer to Fig. 2), thus  $\mu^p$  and  $\sigma^p$  could be inaccurate when compared to the global statistics of a batch in the training course. In PBN, we further combine the globally accumulated statistics ( $\hat{\mu}$  and  $\hat{\sigma}$ , as seen in Alg. 1) with the raw statistics ( $\mu^p$  and  $\sigma^p$ ) together, as inspired by [48]. The final statistics of each patch can be updated as:

$$\begin{aligned} \mu_i^p &= \lambda \mu_i^p + (1 - \lambda) \hat{\mu}_i, \\ \sigma_i^p &= \lambda \sigma_i^p + (1 - \lambda) \hat{\sigma}_i. \end{aligned} \quad (7)$$

During the training stage, we randomly select the number of patches from a set  $\mathbf{S}$  (e.g.,  $\{1, 2, 4\}$ ) for each channel separately. To reduce computational costs, feature maps are not randomly divided into patches independently, which requires  $C$  iterations in a batch. Instead, the feature maps are grouped into  $G$  groups based on the number of patches in the channel dimension, and random patch splits are applied to each group. Therefore, only  $G$  iterations are required. The detailed forward process of the proposed PBN is described in Alg. 1. *During inference, the globally accumulated statistics ( $\hat{\mu}$  and  $\hat{\sigma}$ ) are utilized to normalize feature maps, which is the same as BN.*

**Remark.** The proposed PBN has an advantage over the conventional BN in that it can sufficiently explore the discrepancies between local patches within an image, which allows for the information of diverse data to optimize the BN parameters. Furthermore, the generated diverse information from PBN can also enhance the robustness of other parameters in the model, especially when dealing with cross-domain shifts. Additionally, randomly splitting all pixels of feature maps (i.e.,  $H \times W$   $N$ -d vectors for each channel) into multiple groups and normalizing each group separately does not retain the local structural information in each group, resulting in less noticeable discrepancies. In the experimental section, we conduct experiments to confirm the importance of using the patch structure.

---

**Algorithm 1** The forward process of the proposed PBN

---

- 1: **Input:** Feature maps  $f$  of all samples in a batch.
  - 2: **Output:** The normalized feature maps  $\hat{f}$ .
  - 3: **Initialization:** Initialize the  $\lambda$  in Eq. 7, the set  $\mathbf{S}$  of the number of patches and the globally accumulated statistics ( $\hat{\mu}$  and  $\hat{\sigma}$ ) by the pre-trained model.
  - 4: Compute the global statistics ( $\mu$  and  $\sigma$ ) as Eqs. 2 and 3.
  - 5: Update the accumulated statistics ( $\hat{\mu}$  and  $\hat{\sigma}$ ) as:  
 $\hat{\mu} = (1 - m)\hat{\mu} + m\mu$  and  $\hat{\sigma} = (1 - m)\hat{\sigma} + m\sigma$ .  
*/\* The momentum  $m$  for the globally accumulated statistics is set as 0.1 for BN in default. \*/*
  - 6: Randomly select the number of patches ( $P$ ) from the set  $\mathbf{S}$  for each channel.
  - 7: Group these feature maps according to the number of patches in the channel dimension to form  $G$  groups.
  - 8: **for**  $i \in [1, \dots, G]$  **do**
  - 9:   Randomly split feature maps into  $P$  patches.
  - 10:   **for**  $j \in [1, \dots, P]$  **do**
  - 11:     Compute the raw  $\mu^p$  and  $\sigma^p$  as Eqs. 5 and 6.
  - 12:     Update  $\mu^p$  and  $\sigma^p$  as Eq. 7.
  - 13:     Conduct the normalization as Eq. 4.
  - 14:   **end for**
  - 15: **end for**
  - 16: Regroup all patches together to obtain the normalized feature maps  $\hat{f}$  according to their original positions.
- 

## IV. EXPERIMENTS

### A. Experiments on Classification

In the classification task, we will first introduce the classification datasets and implementation details. Then, we will conduct experiments to compare our method with state-of-the-art methods. Additionally, we will perform ablation studies and further analysis to reveal the properties of our patch-aware batch normalization.

1) *Datasets and Implementation Details:* **Datasets:** In the classification task, we use PACS [49] and CIFAR-10 [50] to perform experiments. PACS [49] consists of four different domains: Photo, Art, Cartoon and Sketch. It contains 9,991 images with 7 object categories in total, including Photo (1,670 images), Art (2,048 images), Cartoon (2,344 images), and Sketch (3,929 images). CIFAR-10 [50] contains small  $32 \times 32$  natural RGB images with respect to 10 categories, with 50,000 training images and 10,000 testing images. In order to validate the robustness of the trained model, we evaluate on CIFAR-10-C [51], which is constructed by corrupting the original CIFAR test sets. For the dataset, there are a total of fifteen noise, including blur, weather, and digital corruption types, and each of them appears at five severity levels or intensities. We follow the setting in [18] to report the averaged performance over all corruptions and intensities.

**Implementation Details:** For the PACS dataset, we follow the same setting as in [23, 9], where we use ResNet-18 as the backbone. *It is worth noting that we use the same baseline (i.e., ERM in all tables) as EFDMix [9].* We report the averaged results five times. In the case of CIFAR-10, we use Wide ResNet as the backbone as done as in [18]. Since our

PBN can be integrated into most existing SOTA methods, we directly replace all BNs of the backbone with our PBN based on the available codes provided by their authors. Therefore, the experimental settings, including learning rate, optimizer, the number of epochs, and the final model selection, are completely consistent with the compared methods.

2) *Comparison with SOTA Methods:* We compare our method with several state-of-the-art (SOTA) methods, including RSC [29], ADA [41], ME-ADA [18], EFDMix [9], NP+ [52], ALT [53] and XDED [23], and integrate our PBN into these methods by replacing BN of the backbone. The experimental results, reported in Tab. I, show that incorporating our method consistently improves performance across all methods. For example, compared with recent methods such as EFDMix [9] and XDED [23], using PBN can increase their performance by +2.9% (57.3 vs. 54.4) and +2.3% (68.8 vs. 66.5), respectively, demonstrating the effectiveness of our proposed PBN. We also report experimental results for the “CIFAR-10 → CIFAR-10-C” task, which show that integrating our method into these existing SOTA methods can also achieve further improvements, as illustrated in Fig. 3.

TABLE I: Comparison with SOTA methods on PACS. We list the result when using Photo (P), Art (A), Cartoon (C), and Sketch (S) as the test domain respectively. For example, P denotes the averaged result of A → P, C → P and S → P. Note that “ERM” is the baseline, *i.e.*, the raw ResNet-18 [1] with the cross-entropy loss.

Method	P	A	C	S	Avg
ERM	34.0	58.6	66.4	27.5	46.6
ERM+PBN	<b>36.2</b>	<b>60.5</b>	<b>69.1</b>	<b>31.5</b>	<b>49.3</b>
RSC [29]	57.3	75.3	77.4	45.9	64.0
RSC+PBN	55.2	<b>76.8</b>	<b>78.5</b>	<b>57.0</b>	<b>66.9</b>
ADA [41]	33.6	59.7	67.1	<b>27.3</b>	46.9
ADA+PBN	<b>36.9</b>	<b>61.5</b>	<b>69.1</b>	26.6	<b>48.5</b>
ME-ADA [18]	33.6	59.7	67.1	26.8	46.8
ME-ADA+PBN	<b>37.1</b>	<b>61.0</b>	<b>68.9</b>	<b>28.2</b>	<b>48.8</b>
EFDMix [9]	42.5	63.2	<b>73.9</b>	38.1	54.4
EFDMix+PBN	<b>49.1</b>	<b>66.9</b>	73.0	<b>40.1</b>	<b>57.3</b>
NP+ [52]	37.9	65.2	61.7	41.5	51.6
NP+PBN	<b>43.3</b>	<b>67.9</b>	<b>62.7</b>	<b>42.0</b>	<b>53.9</b>
ALT [53]	54.6	74.9	75.5	51.0	64.0
ALT+PBN	<b>57.6</b>	<b>76.0</b>	<b>76.3</b>	<b>53.5</b>	<b>65.9</b>
XDED [23]	59.1	76.5	77.2	53.1	66.5
XDED+PBN	<b>62.2</b>	<b>78.3</b>	<b>79.9</b>	<b>54.6</b>	<b>68.8</b>

We also compare our method with the normalization based methods, including CNSN [44], DSU [21] and pAdaIN [20]. The experimental results are listed in Tab. II. As observed in this table, our method outperforms these compared methods. For example, compared with DSU, the performance of our PBN increases it by +2.4% (49.3 vs. 46.9). It is worth noting that, our PBN slightly outperforms pAdaIN, but our method can be integrated into it and further improve its performance. Most normalization based methods aim to introduce extra and diverse information into instance normalization, while our proposed method is an improved batch normalization that can be easily integrated into existing methods by replacing batch normalization with our patch-aware batch normalization. This allows for the combination of the advantages of different normalization methods, leading to improved performance on

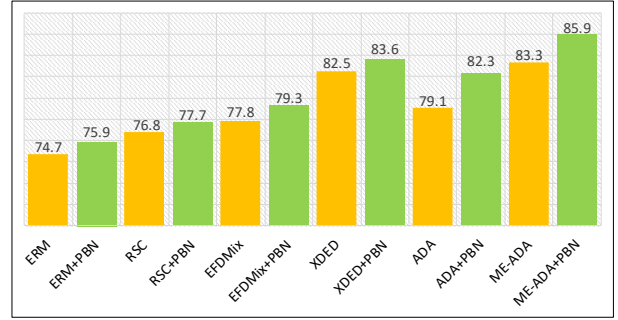


Fig. 3: The experimental results of our PBN and recently SOTA methods in the “CIFAR-10 → CIFAR-10-C” task. Note that “ERM” is the baseline, *i.e.*, the raw Wide ResNet [54] with the cross-entropy loss.

various tasks.

TABLE II: Comparison with the normalization based methods in the image classification task on PACS. In this table, the **bold** is the best performance.

Method	P	A	C	S	Avg
CNSN [44]	31.6	<b>61.7</b>	66.1	20.2	44.9
DSU [21]	33.8	58.8	67.2	27.9	46.9
pAdaIN [20]	35.6	60.5	68.0	30.6	48.7
PBN (Ours)	<b>36.2</b>	60.5	<b>69.1</b>	<b>31.5</b>	<b>49.3</b>
CNSN+PBN	<b>38.3</b>	<b>62.2</b>	65.4	27.9	48.5
DSU+PBN	36.3	61.2	69.0	29.5	49.0
pAdaIN+PBN	38.1	61.3	<b>69.3</b>	<b>29.6</b>	<b>49.6</b>

3) *Ablation Studies and Further Analysis: Ablation studies.* In section III-B, we leverage the globally accumulated statistic to mitigate the instability of the statistics from each patch in the training stage. Here, we perform the experiment to validate the effectiveness of both the module in PBN and PBN without the module, as shown in Tab. III. As seen in this table, our method without the globally accumulated statistics (*i.e.*, “ERM+PBN w/o GS” in Tab. III) can still improve the performance of the baseline (*i.e.*, “ERM”) by +2.2% (48.8 vs. 46.6). Furthermore, when integrating the globally accumulated statistic into PBN, our method can obtain the further improvement, which demonstrates the necessity of the the globally accumulated statistic in PBN. In addition, in order to sufficiently validate the effectiveness of each component in our method, we will also do ablation studies in the other tasks.

TABLE III: Ablation studies in the image classification task on PACS. “w/o” denotes “without”, and “GS” indicates the globally accumulated statistic, *i.e.*,  $\hat{\mu}$  and  $\hat{\sigma}$  in Eq. 7.

Method	P	A	C	S	Avg
ERM	34.0	58.6	66.4	27.5	46.6
ERM+PBN w/o GS	<b>36.3</b>	<b>60.5</b>	<b>69.3</b>	29.0	48.8
ERM+PBN	36.2	<b>60.5</b>	69.1	<b>31.5</b>	<b>49.3</b>

**Evaluation of different splitting schemes and the number of patches.** In this experiment, we present the results of different splitting schemes and the number of patches used on PACS, as shown in Tab. IV. It’s important to note that

to observe the influence of different splitting schemes and patch numbers, we use the same scheme across all feature map channels. For the random splitting scheme, we ensure that each patch is not too small by randomly selecting a position between 1/3 height (or width) and 2/3 height (or width) for 2 and 4 patches. For 9 patches, we select two positions (*i.e.*, 1/5 to 2/5 and 3/5 to 4/5) in both height and width dimensions. As can be seen in the table, the random splitting scheme generally outperforms the equal splitting scheme. Additionally, we find that randomly splitting feature maps into 4 patches (*i.e.*, “P4-random”) achieves the best results.

TABLE IV: Results of different splitting schemes and the number of patches on PACS. In this table, the notation “P2” represents splitting feature maps into two patches. “LR” and “UD” represent splitting feature maps into left-right and up-down patches, respectively. “Equal” indicates that all patches are of the same size, while “random” indicates that feature maps are randomly divided into different patches.

Method	P	A	C	S	Avg
Baseline	34.0	58.6	66.4	27.5	46.6
P2-LR-equal	34.9	59.5	68.3	27.6	47.6
P2-UD-equal	35.5	60.5	67.7	27.2	47.7
P2-LR-random	35.7	60.7	<b>69.5</b>	29.0	48.7
P2-UD-random	36.4	60.9	68.2	29.0	48.6
P4-equal	35.6	60.4	68.0	28.8	48.2
<b>P4-random</b>	<b>36.7</b>	<b>61.4</b>	68.9	29.2	<b>49.1</b>
P9-equal	34.2	60.4	65.8	<b>33.0</b>	48.4
P9-random	34.6	61.1	66.6	31.3	48.4

### Comparison with the pixel based scheme.

In this experiment, we further explore the necessity of using patches in our method. We conduct this experiment using a pixel based scheme, which randomly splits all pixels of a batch (*i.e.*,  $H \times W$   $N$ -dimensional vectors for each channel) into multiple pixel groups. To have a fair comparison, the number of pixel groups is the same as the number of divided patches, and the size of each group is generated by the same random scheme as the patch splitting scheme (*i.e.*, “P4-random” in Tab. IV). The experimental results are listed in Tab. V. As shown, the patch-based scheme is necessary and meaningful in our method, while the pixel based scheme neglects the structural information in the spatial dimension. The differences across local patches can be leveraged to alleviate overfitting to the training set in cross-domain tasks.

TABLE V: Experimental results of the patch based scheme and the pixel based scheme via “P4-random” in Tab. IV .

Method	P	A	C	S	Avg
BN (Baseline)	34.0	58.6	66.4	27.5	46.6
Pixel	34.6	60.4	67.9	24.7	46.9
Patch	<b>36.7</b>	<b>61.4</b>	<b>68.9</b>	<b>29.2</b>	<b>49.1</b>

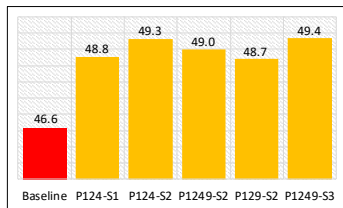


Fig. 4: The analysis of the randomness along the channel dimension. In this figure, “P124-S2” denotes that we randomly select 2 digits from  $\{1, 2, 4\}$  as the number of patches.

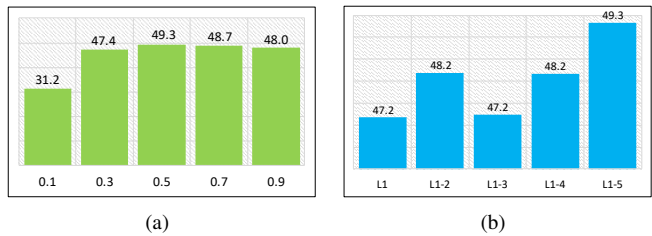


Fig. 5: The analysis of the hyper-parameter  $\lambda$  in Eq. 7 in (a). (b) is the result of using our method at different positions of the backbone. Both (a) and (b) are conducted on PACS.

**The analysis of the randomness along the channel.** To analyze the necessity of randomness on the channel dimension, we conduct experiments using different numbers of patch sets and randomly select numbers, as shown in Fig. 4. As observed in the figure, the “P124-S2” setting achieve good performance, and adding the set size and randomly selected number slightly increased performance. Considering that choosing a more complex setup only brings slight improvements, we opt for a relatively simple setup, which also yields good results. Therefore, we select “P124-S2” as our final setting for classification.

**Evaluation of the impact of our method at different positions.** ResNet consists of five modules, *i.e.*, a convolutional module and four residual block modules. In Fig. 5 (b), we give the experimental result when using our PBN at different positions. In this figure, “L1-5” indicates that we replace all BNs of five modules. As seen, when replacing all raw BNs with PBN, our method can obtain the best result on PACS. In the classification task, we utilize this setting to conduct all experiments.

**The analysis of the hyper-parameter.** In Eq. 7, the hyper-parameter  $\lambda$  is used to balance the influence of the globally accumulated statistics and the statistics of each patch. We analyze the effect of different values of  $\lambda$ , as shown in Fig. 5 (a). From the figure, it can be observed that the best performance is achieved when  $\lambda$  is set to 0.5. Moreover, there is a significant decrease in performance when using only the globally accumulated statistics, as this method reduces the diversity of information.

**Results based on ResNet-50.** To further validate the effectiveness of our method, we also use ResNet-50 as the backbone to conduct the experiment on PACS. The experimental results are listed in Tab. VI. For example, when integrating our PBN into EFDMix [9], it can still increase +2.8% (64.0 vs. 61.2). *We also conduct the ablation based on VGG [55], and put the result in the supplementary materials.*

TABLE VI: Experimental results of using ResNet-50 as the backbone on PACS.

Method	P	A	C	S	Avg
ERM	38.0	63.5	69.2	31.4	50.5
ERM+PBN	<b>41.4</b>	<b>67.0</b>	<b>71.5</b>	<b>38.0</b>	<b>54.5</b>
EFDMix [9]	48.0	75.3	77.4	44.2	61.2
EFDMix+PBN	<b>55.3</b>	<b>78.2</b>	<b>75.9</b>	<b>46.4</b>	<b>64.0</b>

## B. Generalization on Object Detection

**Dataset:** We employ the Diverse-Weather dataset [42] to conduct the experiment in the object detection task. It consists of five scenes with different weather conditions, *i.e.*, daytime-sunny, night-sunny, dusk-rainy, night-rainy, and daytime-foggy. Particularly, the daytime-sunny scene is the source domain for training, and the night-sunny, dusk-rainy, night-rainy, and daytime-foggy scenes are target domains for testing. For the daytime-sunny scene, 19,395 images are for training. The night-sunny, dusk-rainy, night-rainy, and daytime-foggy scenes separately include 26,158, 3,501, 2,494, and 3,775 images for test.

**Implementation details:** For the Diverse-Weather dataset, we train our model on the daytime-sunny domain and evaluate it on other domains. In contrast to the classification task, the object detection task involves identifying small objects, so we retain the batch normalization (BN) layer in the last two ResNet blocks and replace the other BNs with the proposed PBNs. We implement our method based on the available codes provided by the authors of the SOTA methods and adapt them to our method.

TABLE VII: Comparison with SOTA methods in the object detection task. The model is trained on daytime-sunny and test on Night-Sunny (NS), Dusk-Rainy (DR), Night-Rainy (NR) and Daytime-Foggy (DF), respectively.

Method	NS	DR	NR	DF	Avg
CycConf [56]	<b>45.2</b>	36.0	15.7	38.3	33.8
CycConf+PBN	44.8	<b>40.8</b>	<b>19.6</b>	<b>38.9</b>	<b>36.0</b>
CSD [42]	37.4	27.2	12.9	33.3	27.7
CSD+PBN	<b>38.1</b>	<b>28.4</b>	<b>14.0</b>	<b>32.6</b>	<b>28.3</b>
Faster R-CNN [6]	46.8	37.5	16.7	38.1	34.8
Faster R-CNN+PBN	<b>47.0</b>	<b>44.3</b>	<b>23.8</b>	<b>40.4</b>	<b>38.9</b>

TABLE VIII: Ablation studies in the object detection task. “w/o” denotes “without”, and “GS” indicates the globally accumulated statistic, *i.e.*,  $\hat{\mu}$  and  $\hat{\sigma}$  in Eq. 7.

Method	NS	DR	NR	DF	Avg
Faster R-CNN (FR)	46.8	37.5	16.7	38.1	34.8
FR+PBN w/o GS	<b>47.0</b>	43.7	23.0	40.1	38.5
FR+PBN	<b>47.0</b>	<b>44.3</b>	<b>23.8</b>	<b>40.4</b>	<b>38.9</b>
YOLOV5	33.5	25.5	10.4	38.1	26.9
YOLOV5+PBN	<b>35.9</b>	<b>27.2</b>	<b>13.9</b>	<b>43.0</b>	<b>30.0</b>

**Results:** In this section, we compare our patch-aware batch normalization with some recently proposed state-of-the-art single-domain generalized object detection methods, such as CycConf [56] and CSD [42]. The experimental results are shown in Tab. VII. As can be seen, using our method consistently improves the performance of SOTA methods. It is also worth noting that Faster R-CNN [6] is implemented using the Detectron2 [57] library, which includes the FPN module [58]. Thus, Faster R-CNN achieves better results than other methods.

We also conduct experiments on the object detection task to validate the effectiveness of the module in our PBN, as reported in Tab. VIII. Conducting patch-aware batch normalization (*i.e.*, “FR+PBN w/o GS” in Tab. VIII) can improve the performance by +3.7% (38.5 vs. 34.8) compared to Faster

R-CNN. Moreover, our method can be further improved by combining the globally accumulated statistics with the patch-wise statistics (*i.e.*, “FR+PBN” in Tab. VIII). Besides, we integrate our PBN into YOLOv5s, as shown in Tab. VIII, indicate that using our PBN in YOLO can enhance the original generalization performance of YOLO.

## C. Generalization on Instance Retrieval

We conduct an experiment on an instance retrieval task, namely Person Re-identification (Re-ID), which aims to learn generalizable features for matching images of the same identity from different cameras [59]. We use Person Re-ID datasets, such as Market1501 [60] and GRID [61], to conduct cross-domain instance retrieval. We employ OSNet [62] as the backbone and follow the experiment protocol of [9]. Similar to our findings in classification and object detection tasks, when our PBN was added to existing SOTA methods, their performance consistently improved, as shown in Tab. IX. This further validates the effectiveness of using our PBN to mitigate the overfitting to the training set in cross-domain tasks.

## D. Generalization on Semantic Segmentation

In the semantic segmentation task, we conduct the multi-domain generalization experiment as in [11]. We train all methods on the Cityscapes dataset [63], which consists of multiple domains, and show their performance on other datasets, including BDD-100K [64], Mapillary [65], GTAV [66], and SYNTHIA [67], to measure the generalization capability on unseen domains.

In this section, we adopt DeepLabV3+ [7] as the backbone, following the setting in [11]. We compare our method with RobustNet [11], which disentangles the domain-specific style and domain-invariant content encoded in higher-order statistics (*i.e.*, feature covariance) of the feature representations and selectively removes only the style information causing domain shift. The experimental results are reported in Tab. X. As can be seen in the table, RobustNet improves the performance of the Baseline, and plugging our PBN into the RobustNet can further generate better results. Additionally, we conduct an ablation study in the semantic segmentation task, as shown in Tab. XI, which validates the efficacy of using the patch-aware normalization and globally accumulated statistics.

## E. Further Analysis

1) *Visualization of Statistics:* We have generated a visualization of the differences between local patches within an image, as shown in Fig. 6. To obtain this visualization, we compute the statistics of feature maps before the first batch normalization (BN) layer of ResNet [1], resulting in  $(\mu, \sigma)$  where  $\mu$  and  $\sigma$  are vectors of length  $C$  (*i.e.*, the number of channels), and in this case,  $C$  is 64. As can be seen in Fig. 6 (b), there are obvious differences in the standard deviations between the different patches, while the mean values are only slightly different. We also show that different partitions with varying sizes can introduce additional discrepancies, which is beneficial for mitigating the impact of overfitting.

TABLE IX: Comparison with some SOTA methods in the instance retrieval task. We run experiment three times and report the averaged result and standard deviation on Market1501 and GRID, respectively.

Method	Market1501→GRID				GRID→Market1501			
	mAP	R1	R5	R10	mAP	R1	R5	R10
Baseline	33.3±0.4	24.5±0.4	42.1±1.0	48.8±0.7	3.9±0.4	13.1±1.0	25.3±2.2	31.7±2.0
MixStyle [45]	33.8±0.9	24.8±1.6	<b>43.7±2.0</b>	53.1±1.6	4.9±0.2	15.4±1.2	28.4±1.3	35.7±0.9
MixStyle+PBN	<b>35.9±2.3</b>	<b>28.0±2.3</b>	43.2±4.2	<b>52.5±1.3</b>	<b>5.6±0.7</b>	<b>16.9±1.6</b>	<b>30.5±3.1</b>	<b>37.8±3.4</b>
EFDMix [9]	35.5±1.8	26.7±3.3	44.4±0.8	<b>53.6±2.0</b>	6.4±0.2	19.9±0.6	34.4±1.0	42.2±0.8
EFDMix + PBN	<b>37.0±0.9</b>	<b>28.0±2.0</b>	<b>44.8±0.7</b>	<b>53.6±1.1</b>	<b>6.8±0.3</b>	<b>20.5±0.5</b>	<b>35.4±0.9</b>	<b>43.1±0.8</b>

TABLE X: Experimental results of the model trained using Cityscapes on BDD-100K (B), Mapillary (M), GTAV (G) and SYNTHIA (S) in the semantic segmentation task.

Method	B	M	G	S	Avg
Baseline	44.5	53.0	41.4	24.3	40.8
RobustNet [11]	48.7	57.0	44.4	25.7	44.0
RobustNet+PBN	<b>50.6</b>	<b>57.8</b>	<b>46.6</b>	<b>26.2</b>	<b>45.3</b>

TABLE XI: Ablation studies in semantic segmentation. “C” denotes the training set, *i.e.*, Cityscapes. “w/o” denotes “without”, and “GS” is the globally accumulated statistic, *i.e.*,  $\hat{\mu}$  and  $\hat{\sigma}$  in Eq. 7.

Method	B	M	G	S	Avg
Baseline (BL)	44.5	53.0	41.4	24.3	40.8
BL+PBN w/o GS	<b>46.2</b>	53.7	<b>43.5</b>	25.3	42.2
BL+PBN	46.1	<b>57.2</b>	42.7	<b>25.4</b>	<b>42.9</b>

2) *Comparison to those BN, LN, IN and GN*: In Tab. XIII, we compare our method with other typical normalizations. As observed, our PBN achieves superior performance compared to the alternatives. It is worth noting that IN shows poor performance due to its limitation in eliminating discriminative patterns that might be beneficial for a specific instance, as stated in the abstract of the literature.

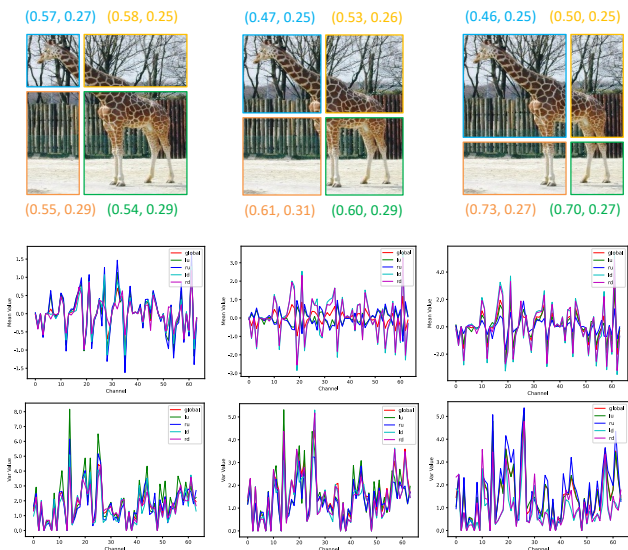
3) *Experiments based on ViT*: We extend our method to Layer Normalization (referred to as PLN) using the ViT and present the experimental results in Tab. XIV. Additionally, we have partitioned the patch dimension of the features using the P4-random method. As evident, this extension also contributes to an improvement in the performance of ViT.

Method	Accuracy
ADA [41]	69.8
ADA+PBN	<b>77.0</b>
ME-ADA [18]	76.9
ME-ADA+PBN	<b>82.4</b>
BL	69.3
BL+PBNw/o GS	74.3
BL+PBN	<b>74.9</b>

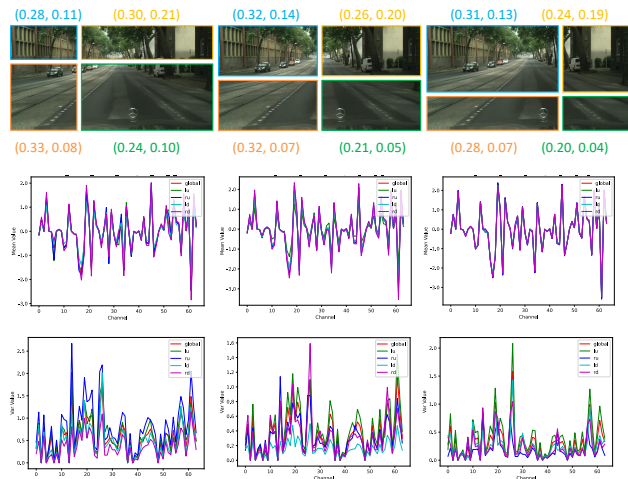
4) *Experiments based on Other Backbones*: We also add the experiment based on VGG [55] on PACS in Tab. XIII and DenseNet [68] on CIFAR-10 in Tab. XII, respectively. As

TABLE XIII: The experimental results of our PBN on VGG on the PACS dataset.

Method	P	A	C	S	Avg
Baseline(BL)	60.4	63.5	38.9	28.6	47.8
BL+PBN w/o GS	<b>60.9</b>	65.6	39.8	32.1	49.6
BL+PBN	60.0	<b>66.0</b>	<b>39.9</b>	<b>33.6</b>	<b>49.9</b>



(a) Images for classification.



(b) Images for detection and segmentation.

Fig. 6: Visualization of differences between non-overlapping patches within an image. In this figure, “lu”, “ru”, “ld” and “rd” indicate the position of each patch, where “lu” stands for the left-upper patch, “ru” for the right-upper patch, “ld” for the left-down patch, and “rd” for the right-down patch. Each curve in the figure represents mean or standard deviation of a patch. “global” indicates the global statistics. The second and third rows are the mean ( $\mu$ ) and standard deviation ( $\sigma$ ).

observed in the tables, our PBN consistently demonstrates its effectiveness with different backbones, which further confirm



TABLE XIV: Performance assessment on the PACS dataset: leveraging a model founded on the ViT architecture.

Method	P	A	C	S	Avg
ViT-small	64.5	64.7	39.8	50.9	55.0
ViT-small+PLN	<b>66.3</b>	<b>65.9</b>	<b>44.2</b>	<b>50.9</b>	<b>56.8</b>
ViT-large	72.5	74.8	48.1	75.8	67.8
ViT-large+PLN	<b>73.4</b>	<b>77.2</b>	<b>48.2</b>	<b>78.3</b>	<b>69.3</b>

TABLE XIII: Experiments on the PACS Dataset with previous normalization methods.

Method	P	A	C	S	Avg
BN	58.6	66.4	34.0	27.5	46.6
IN	23.8	16.3	17.2	11.8	17.3
LN	54.4	48.4	20.5	28.4	37.9
GN	58.0	52.6	32.9	<b>44.9</b>	47.1
PBN	<b>60.5</b>	<b>69.1</b>	<b>36.2</b>	31.5	<b>49.3</b>

the efficacy of our Patch-aware Batch Normalization.

TABLE XVI: Combining PBN with various augmentation methods on the PACS dataset to validate the stability and scalability of PBN

Method	P	A	C	S	Avg
Strong_Aug	61.3	70.8	37.6	40.9	52.7
PBN w Strong_Aug	<b>63.5</b>	<b>73.0</b>	<b>38.5</b>	<b>42.2</b>	<b>54.3</b>
RandAug	65.3	71.1	42.0	49.0	56.8
PBN w RandAug	<b>68.9</b>	<b>72.5</b>	<b>44.1</b>	<b>50.0</b>	<b>58.9</b>
AutoAug	61.0	71.2	40.3	54.9	56.9
PBN w AutoAug	<b>64.8</b>	<b>72.1</b>	<b>42.0</b>	<b>55.7</b>	<b>58.6</b>

5) *The stability and sensitivity of PBN:* Based on different augmentations, we use PBN for experiment, as shown in Tab. XVI. Our PBN still keeps the stable improvement.

6) *Experiments on the larger-scale datasets:* We extend our validation of the effectiveness of the PBN to larger-scale datasets, including ImageNet-C, ImageNet-A, and Stylized-ImageNet (Sty-IN), as presented in Tab. XVII. Across these diverse and challenging datasets, our PBN consistently outperforms the baseline model without PBN, demonstrating its robustness and generalization capabilities. The improvements in performance are particularly noteworthy on ImageNet-C and ImageNet-A, which contain various corruptions and natural adversarial examples, respectively. This highlights the ability of PBN to enhance model robustness against distribution shifts and adversarial perturbations. Additionally, the promising results on Stylized-ImageNet, which features stylized renditions of natural images, showcase the effectiveness of PBN in handling diverse visual domains. The aforementioned experimental results convincingly establish the applicability and versatility of PBN on large-scale datasets, solidifying its potential for widespread adoption in real-world computer vision applications.

7) *Evaluation on the training time.:* We measure the time required to train for one epoch using the original baseline method and our integrated method, as shown in Tab. XVIII. Our proposed method only slightly increases the training time compared to the baseline. This is because our method involves new statistical calculations only in the BN layer and does not affect other layers in the backbone.

8) *Comparison with Meta-BIN.:* We compare our proposed method with Meta-BIN in the DG-ReID setting, and our method can achieve better performance, as shown in Tab. XIX.

TABLE XVII: Experimental evaluation on ImageNet (ImN). ImageNet is source domain, and we test the model in different domains. It is worth noting that for mCE, the smaller value is better; for Top-1 ACC, the larger value is better. ‘‘R50’’ is the ResNet-50.

Method	ImN-C (mCE)	ImN-A (Top-1 Acc)
R50	74.8	3.1
R50+PBN	<b>68.3</b> ↓ <b>6.5</b>	<b>6.1</b> ↑ <b>3.0</b>
R50+AuxBN[69]	69.7	4.8
R50+AuxBN+PBN	<b>66.5</b> ↓ <b>3.2</b>	<b>7.0</b> ↑ <b>2.2</b>
Method	Sty-ImN (Top-1 Acc)	ImN (Top-1 Acc)
R50	8.0	76.6
R50+PBN	<b>11.6</b> ↑ <b>3.6</b>	<b>77.7</b> ↑ <b>1.1</b>
R50+AuxBN[69]	10.3	77.5
R50+AuxBN+PBN	<b>13.4</b> ↑ <b>3.1</b>	<b>77.9</b> ↑ <b>0.4</b>

TABLE XVIII: The training times (second) of our method.

Method	Time/Epoch
ResNet18	5.0483
PBN-ResNet18	5.1738
ResNet50	9.3048
PBN-ResNet50	9.5886

Compared to Meta-BIN, our method can bring more diverse information.

TABLE XIX: Comparison between MetaBIN and our PBN in the DG-ReID setting.

Method	M→G		G→M	
	mAP	R1	mAP	R1
MetaBIN [70]	34.05	24.84	4.26	13.45
PBN	<b>35.67</b>	<b>26.93</b>	<b>4.43</b>	<b>13.53</b>

## V. CONCLUSION

In this paper, we propose a novel method called patch-aware batch normalization (PBN) for enhancing cross-domain robustness by exploiting the differences between local patches within an image to alleviate overfitting issues. PBN divides feature maps into different patches and performs normalization operations independently, leading to better optimization of the BN parameters. Additionally, globally accumulated statistics are integrated to mitigate the inaccuracy of patch statistics. Multiple experiments on different tasks validate the effectiveness of our proposed PBN.

In our experiments, we also attempt to apply our method to the multi-domain generalization classification task, but it does not result in significant improvements. In contrast to the cityscapes dataset, there may be significant differences across multiple domains in the multi-domain generalized classification task, which can introduce diverse information when randomly selecting images to form each batch. For instance, on the PACS dataset, where we use Photo (P), Art (A), and Sketch (S) to train the model, the domain gap is large in the training set. Using our method in this scenario could introduce more randomness that may act as noise during training, because we observe that using our PBN leads to a larger standard deviation than the baseline. We will investigate this issue in future work.

## REFERENCES

- [1] K. He, X. Zhang, S. Ren, and J. Sun, "Deep residual learning for image recognition," in *IEEE Conference on Computer Vision and Pattern Recognition (CVPR)*, 2016, pp. 770–778.
- [2] Z. Li, H. Tang, Z. Peng, G.-J. Qi, and J. Tang, "Knowledge-guided semantic transfer network for few-shot image recognition," *IEEE Transactions on Neural Networks and Learning Systems (TNNLS)*, 2023.
- [3] Z. Zha, H. Tang, Y. Sun, and J. Tang, "Boosting few-shot fine-grained recognition with background suppression and foreground alignment," *IEEE Transactions on Circuits and Systems for Video Technology (TCSVT)*, vol. 33, no. 8, pp. 3947–3961, 2023.
- [4] H. Tang, C. Yuan, Z. Li, and J. Tang, "Learning attention-guided pyramidal features for few-shot fine-grained recognition," *Pattern Recognition (PR)*, vol. 130, p. 108792, 2022.
- [5] R. Yan, L. Xie, X. Shu, L. Zhang, and J. Tang, "Progressive instance-aware feature learning for compositional action recognition," *IEEE Transactions on Pattern Analysis and Machine Intelligence (TPAMI)*, vol. 45, no. 8, pp. 10317–10330, 2023.
- [6] S. Ren, K. He, R. B. Girshick, and J. Sun, "Faster R-CNN: towards real-time object detection with region proposal networks," in *Advances in Neural Information Processing Systems (NeurIPS)*, 2015, pp. 1137–1149.
- [7] L. Chen, Y. Zhu, G. Papandreou, F. Schroff, and H. Adam, "Encoder-decoder with atrous separable convolution for semantic image segmentation," in *European Conference on Computer Vision (ECCV)*, 2018, pp. 801–818.
- [8] Z. Li, Y. Sun, L. Zhang, and J. Tang, "Ctnet: Context-based tandem network for semantic segmentation," *IEEE Transactions on Pattern Analysis and Machine Intelligence (TPAMI)*, vol. 44, no. 12, pp. 9904–9917, 2021.
- [9] Y. Zhang, M. Li, R. Li, K. Jia, and L. Zhang, "Exact feature distribution matching for arbitrary style transfer and domain generalization," in *IEEE Conference on Computer Vision and Pattern Recognition (CVPR)*, 2022, pp. 8035–8045.
- [10] J. Zhang, L. Qi, Y. Shi, and Y. Gao, "MVDG: A unified multi-view framework for domain generalization," in *European Conference on Computer Vision (ECCV)*, 2022, pp. 161–177.
- [11] S. Choi, S. Jung, H. Yun, J. T. Kim, S. Kim, and J. Choo, "Robustnet: Improving domain generalization in urban-scene segmentation via instance selective whitening," in *IEEE Conference on Computer Vision and Pattern Recognition (CVPR)*, 2021, pp. 11580–11590.
- [12] J. Guo, N. Wang, L. Qi, and Y. Shi, "Aloft: A lightweight mlp-like architecture with dynamic low-frequency transform for domain generalization," in *IEEE Conference on Computer Vision and Pattern Recognition (CVPR)*, 2023, pp. 24132–24141.
- [13] Z. Chen, W. Wang, Z. Zhao, F. Su, A. Men, and Y. Dong, "Instance paradigm contrastive learning for domain generalization," *IEEE Transactions on Circuits and Systems for Video Technology (TCSVT)*, vol. 34, no. 2, pp. 1032–1042, 2024.
- [14] J. Li, Y. Li, H. Wang, C. Liu, and J. Tan, "Exploring explicitly disentangled features for domain generalization," *IEEE Transactions on Circuits and Systems for Video Technology (TCSVT)*, vol. 33, no. 11, pp. 6360–6373, 2024.
- [15] Y. Zhang, S. Tian, M. Liao, Z. Zhang, W. Zou, and C. Xu, "Fine-grained self-supervision for generalizable semantic segmentation," *IEEE Transactions on Circuits and Systems for Video Technology (TCSVT)*, vol. 34, no. 1, pp. 371–383, 2024.
- [16] X. Fan, Q. Wang, J. Ke, F. Yang, B. Gong, and M. Zhou, "Adversarially adaptive normalization for single domain generalization," in *IEEE Conference on Computer Vision and Pattern Recognition (CVPR)*, 2021, pp. 8208–8217.
- [17] T. Chen, M. Baktashmotlagh, Z. Wang, and M. Salzmann, "Center-aware adversarial augmentation for single domain generalization," in *IEEE Winter Conference on Applications of Computer Vision (WACV)*, 2023, pp. 4157–4165.
- [18] L. Zhao, T. Liu, X. Peng, and D. N. Metaxas, "Maximum-entropy adversarial data augmentation for improved generalization and robustness," in *Advances in Neural Information Processing Systems (NeurIPS)*, 2020, pp. 14435–14447.
- [19] S. Cheng, T. Gokhale, and Y. Yang, "Adversarial bayesian augmentation for single-source domain generalization," in *IEEE International Conference on Computer Vision (ICCV)*, 2023, pp. 11400–11410.
- [20] O. Nuriel, S. Benaim, and L. Wolf, "Permuted adain: Reducing the bias towards global statistics in image classification," in *IEEE Conference on Computer Vision and Pattern Recognition (CVPR)*, 2021, pp. 9482–9491.
- [21] X. Li, Y. Dai, Y. Ge, J. Liu, Y. Shan, and L. Duan, "Uncertainty modeling for out-of-distribution generalization," in *International Conference on Learning Representations (ICLR)*, 2022.
- [22] I. Çugu, M. Mancini, Y. Chen, and Z. Akata, "Attention consistency on visual corruptions for single-source domain generalization," in *IEEE Conference on Computer Vision and Pattern Recognition (CVPR)*, 2022, pp. 4165–4174.
- [23] K. Lee, S. Kim, and S. Kwak, "Cross-domain ensemble distillation for domain generalization," in *European Conference on Computer Vision (ECCV)*, 2022, pp. 1–20.
- [24] X. Huang and S. J. Belongie, "Arbitrary style transfer in real-time with adaptive instance normalization," in *IEEE International Conference on Computer Vision (ICCV)*, 2017, pp. 1501–1510.
- [25] L. A. Gatys, A. S. Ecker, and M. Bethge, "Image style transfer using convolutional neural networks," in *IEEE Conference on Computer Vision and Pattern Recognition (CVPR)*, 2016, pp. 2414–2423.
- [26] W. Chang, T. You, S. Seo, S. Kwak, and B. Han, "Domain-specific batch normalization for unsupervised domain adaptation," in *IEEE Conference on Computer*

- Vision and Pattern Recognition (CVPR)*, 2019, pp. 7354–7362.
- [27] S. Seo, Y. Suh, D. Kim, G. Kim, J. Han, and B. Han, “Learning to optimize domain specific normalization for domain generalization,” in *European Conference on Computer Vision (ECCV)*, 2020, pp. 68–83.
- [28] X. Jin, C. Lan, W. Zeng, and Z. Chen, “Style normalization and restitution for domain generalization and adaptation,” *IEEE Transactions on Multimedia (TMM)*, vol. 24, pp. 3636–3651, 2021.
- [29] Z. Huang, H. Wang, E. P. Xing, and D. Huang, “Self-challenging improves cross-domain generalization,” in *European Conference on Computer Vision (ECCV)*, 2020, pp. 124–140.
- [30] J. Guo, L. Qi, and Y. Shi, “Domaindrop: Suppressing domain-sensitive channels for domain generalization,” in *IEEE International Conference on Computer Vision (ICCV)*, 2023, pp. 19 114–19 124.
- [31] L. Qi, H. Yang, Y. Shi, and X. Geng, “Normaug: Normalization-guided augmentation for domain generalization,” *IEEE Transactions on Image Processing (TIP)*, vol. 33, pp. 1419–1431, 2024.
- [32] Y. Wang, L. Qi, Y. Shi, and Y. Gao, “Feature-based style randomization for domain generalization,” *IEEE Transactions on Circuits and Systems for Video Technology (TCSVT)*, vol. 32, no. 8, pp. 5495–5509, 2022.
- [33] L. Qi, L. Wang, Y. Shi, and X. Geng, “A novel mix-normalization method for generalizable multi-source person re-identification,” *IEEE Transactions on Multimedia (TMM)*, vol. 25, pp. 4856–4867, 2023.
- [34] J. Cha, S. Chun, K. Lee, H. Cho, S. Park, Y. Lee, and S. Park, “SWAD: domain generalization by seeking flat minima,” in *Advances in Neural Information Processing Systems (NeurIPS)*, 2021, pp. 22 405–22 418.
- [35] R. Meng, X. Li, W. Chen, S. Yang, J. Song, X. Wang, L. Zhang, M. Song, D. Xie, and S. Pu, “Attention diversification for domain generalization,” in *European Conference on Computer Vision (ECCV)*, 2022, pp. 322–340.
- [36] R. Yan, M. Z. Shou, Y. Ge, J. Wang, X. Lin, G. Cai, and J. Tang, “Video-text pre-training with learned regions for retrieval,” in *AAAI Conference on Artificial Intelligence (AAAI)*, vol. 37, no. 3, 2023, pp. 3100–3108.
- [37] Y. Ding, L. Wang, B. Liang, S. Liang, Y. Wang, and F. Chen, “Domain generalization by learning and removing domain-specific features,” *arXiv preprint arXiv:2212.07101*, 2022.
- [38] S. Lin, Z. Zhang, Z. Huang, Y. Lu, C. Lan, P. Chu, Q. You, J. Wang, Z. Liu, A. Parulkar, V. Navkal, and Z. Chen, “Deep frequency filtering for domain generalization,” in *IEEE Conference on Computer Vision and Pattern Recognition (CVPR)*, 2023, pp. 11 797–11 807.
- [39] Z. Wang, Y. Luo, R. Qiu, Z. Huang, and M. Bakhtashmotlagh, “Learning to diversify for single domain generalization,” in *IEEE International Conference on Computer Vision (ICCV)*, 2021, pp. 834–843.
- [40] F. Qiao, L. Zhao, and X. Peng, “Learning to learn single domain generalization,” in *IEEE Conference on Computer Vision and Pattern Recognition (CVPR)*, 2020, pp. 12 556–12 565.
- [41] R. Volpi, H. Namkoong, O. Sener, J. C. Duchi, V. Murino, and S. Savarese, “Generalizing to unseen domains via adversarial data augmentation,” in *Advances in Neural Information Processing Systems (NeurIPS)*, 2018.
- [42] A. Wu and C. Deng, “Single-domain generalized object detection in urban scene via cyclic-disentangled self-distillation,” in *IEEE Conference on Computer Vision and Pattern Recognition (CVPR)*, 2022, pp. 847–856.
- [43] C. Wan, X. Shen, Y. Zhang, Z. Yin, X. Tian, F. Gao, J. Huang, and X. Hua, “Meta convolutional neural networks for single domain generalization,” in *IEEE Conference on Computer Vision and Pattern Recognition (CVPR)*, 2022, pp. 4682–4691.
- [44] Z. Tang, Y. Gao, Y. Zhu, Z. Zhang, M. Li, and D. N. Metaxas, “Crossnorm and selfnorm for generalization under distribution shifts,” in *IEEE International Conference on Computer Vision (ICCV)*, 2021, pp. 52–61.
- [45] K. Zhou, Y. Yang, Y. Qiao, and T. Xiang, “Domain generalization with mixstyle,” in *International Conference on Learning Representations (ICLR)*, 2021.
- [46] L. Huang, Y. Zhou, T. Wang, J. Luo, and X. Liu, “Delving into the estimation shift of batch normalization in a network,” in *IEEE Conference on Computer Vision and Pattern Recognition (CVPR)*, 2022, pp. 763–772.
- [47] S. Ioffe and C. Szegedy, “Batch normalization: Accelerating deep network training by reducing internal covariate shift,” in *International Conference on Machine Learning (ICML)*, F. R. Bach and D. M. Blei, Eds., 2015, pp. 448–456.
- [48] Z. Kou, K. You, M. Long, and J. Wang, “Stochastic normalization,” in *Advances in Neural Information Processing Systems (NeurIPS)*, 2020, pp. 16 304–16 314.
- [49] D. Li, Y. Yang, Y.-Z. Song, and T. M. Hospedales, “Deeper, broader and artier domain generalization,” in *IEEE International Conference on Computer Vision (ICCV)*, 2017, pp. 5542–5550.
- [50] A. Krizhevsky, G. Hinton *et al.*, “Learning multiple layers of features from tiny images,” 2009.
- [51] D. Hendrycks and T. G. Dietterich, “Benchmarking neural network robustness to common corruptions and perturbations,” in *International Conference on Learning Representations (ICLR)*, 2019.
- [52] Q. Fan, M. Segu, Y.-W. Tai, F. Yu, C.-K. Tang, B. Schiele, and D. Dai, “Normalization perturbation: A simple domain generalization method for real-world domain shifts,” in *IEEE International Conference on Robotics and Automation (ICRA)*, 2023.
- [53] T. Gokhale, R. Anirudh, J. J. Thiagarajan, B. Kailkhura, C. Baral, and Y. Yang, “Improving diversity with adversarially learned transformations for domain generalization,” in *IEEE Winter Conference on Applications of Computer Vision (WACV)*, 2023, pp. 434–443.
- [54] S. Zagoruyko and N. Komodakis, “Wide residual networks,” in *The British Machine Vision Conference (BMVC)*, 2016.

- [55] K. Simonyan and A. Zisserman, “Very deep convolutional networks for large-scale image recognition,” in *International Conference on Learning Representations (ICLR)*, 2015.
- [56] X. Wang, T. E. Huang, B. Liu, F. Yu, X. Wang, J. E. Gonzalez, and T. Darrell, “Robust object detection via instance-level temporal cycle confusion,” in *IEEE International Conference on Computer Vision (ICCV)*, 2021, pp. 9143–9152.
- [57] Y. Wu, A. Kirillov, F. Massa, W.-Y. Lo, and R. Girshick, “Detectron2,” <https://github.com/facebookresearch/detectron2>, 2019.
- [58] T. Lin, P. Dollár, R. B. Girshick, K. He, B. Hariharan, and S. J. Belongie, “Feature pyramid networks for object detection,” in *IEEE Conference on Computer Vision and Pattern Recognition (CVPR)*, 2017, pp. 2117–2125.
- [59] L. Qi, L. Wang, J. Huo, L. Zhou, Y. Shi, and Y. Gao, “A novel unsupervised camera-aware domain adaptation framework for person re-identification,” in *IEEE International Conference on Computer Vision (ICCV)*, 2019, pp. 8080–8089.
- [60] L. Zheng, L. Shen, L. Tian, S. Wang, J. Wang, and Q. Tian, “Scalable person re-identification: A benchmark,” in *IEEE International Conference on Computer Vision (ICCV)*, 2015, pp. 1116–1124.
- [61] C. C. Loy, T. Xiang, and S. Gong, “Multi-camera activity correlation analysis,” in *IEEE Conference on Computer Vision and Pattern Recognition (CVPR)*, 2009, pp. 1988–1995.
- [62] K. Zhou, Y. Yang, A. Cavallaro, and T. Xiang, “Omni-scale feature learning for person re-identification,” in *IEEE International Conference on Computer Vision (ICCV)*, 2019, pp. 3702–3712.
- [63] M. Cordts, M. Omran, S. Ramos, T. Rehfeld, M. Enzweiler, R. Benenson, U. Franke, S. Roth, and B. Schiele, “The cityscapes dataset for semantic urban scene understanding,” in *IEEE Conference on Computer Vision and Pattern Recognition (CVPR)*, 2016, pp. 3213–3223.
- [64] F. Yu, H. Chen, X. Wang, W. Xian, Y. Chen, F. Liu, V. Madhavan, and T. Darrell, “Bdd100k: A diverse driving dataset for heterogeneous multitask learning,” in *IEEE Conference on Computer Vision and Pattern Recognition (CVPR)*, 2020, pp. 2636–2645.
- [65] G. Neuhold, T. Ollmann, S. Rota Bulo, and P. Kotschieder, “The mapillary vistas dataset for semantic understanding of street scenes,” in *IEEE International Conference on Computer Vision (ICCV)*, 2017, pp. 4990–4999.
- [66] S. R. Richter, V. Vineet, S. Roth, and V. Koltun, “Playing for data: Ground truth from computer games,” in *European Conference on Computer Vision (ECCV)*, 2016, pp. 102–118.
- [67] G. Ros, L. Sellart, J. Materzynska, D. Vazquez, and A. M. Lopez, “The synthia dataset: A large collection of synthetic images for semantic segmentation of urban scenes,” in *IEEE Conference on Computer Vision and Pattern Recognition (CVPR)*, 2016, pp. 3234–3243.
- [68] G. Huang, Z. Liu, L. Van Der Maaten, and K. Q. Weinberger, “Densely connected convolutional networks,” in *IEEE Conference on Computer Vision and Pattern Recognition (CVPR)*, 2017, pp. 11 400–11 410.
- [69] B. Jiao, L. Liu, L. Gao, G. Lin, L. Yang, S. Zhang, P. Wang, and Y. Zhang, “Dynamically transformed instance normalization network for generalizable person re-identification,” in *European Conference on Computer Vision (ECCV)*, 2022, pp. 285–301.
- [70] S. Choi, T. Kim, M. Jeong, H. Park, and C. Kim, “Meta batch-instance normalization for generalizable person re-identification,” in *IEEE conference on Computer Vision and Pattern Recognition (CVPR)*, 2021, pp. 3425–3435.